XLVI CILAMCE
VITÓRIA - ES - BRAZIL - 2025
XLVI IBERO-LATIN AMERICAN CONGRESS ON COMPUTATIONAL METHODS IN ENGENEERING

Virtual tests of hardening porous metallic materials based on computational homogenization

da Maia C. A.[1], Rossi R.[1]

[1]*Departamento de Engenharia Mecânica, Universidade Federal do Rio Grande do Sul*
R. Sarmento Leite 425, 90040-001, Porto Alegre, RS, Brazil
carlosalbertodamaia@gmail.com, rrossi@ufrgs.br

Abstract. This study investigates the apparent mechanical strength of porous metallic materials by performing virtual tests on three-dimensional representative volume elements (RVEs). A key distinction from previous work in literature is the consideration of a hardening metallic matrix, modeled using a bounded Voce-type isotropic hardening law combined with a rate-independent J_2 isotropic hardening plasticity criterion. Each RVE features randomly distributed, non-overlapping spherical voids embedded within an elastoplastic matrix. Distinct macroscopic stress states are obtained by applying mixed boundary conditions and manipulating specific loading parameters. The macroscopic stress, derived as the average of its microscopic counterpart within the RVE, reflects a quasi-asymptotic macroscopic response. The analyses explore the influence of varying porosity levels and isotropic hardening factors, demonstrating their impact on the apparent/macroscopic yield or limit loading locus.

Keywords: Computational Homogenization, Porous Material, RVE, Plasticity, Hardening.

1 Introduction

Porous materials have mechanical and physical properties like high stiffness-to-weight ratio, large specific surface area, and energy absorption capability due to their internal voided microstructure Liu and Chen [1], Banhart et al. [2]. Traditional classifications include closed-cell materials for impact absorbers and open-cell materials for fluid transport applications like filtration, catalytic support, thermal or acoustic insulation, and lubricant reservoirs Binder C. et al. [3]. Processing methods, including powder metallurgy, laser powder bed fusion, and direct energy deposition, can cause uncontrolled porosity, which can compromise structural integrity Ahmed Obeidi et al. [4]. However, intentionally adding voids can improve lightweight components in the automotive, aerospace, and biomedical industries, requiring a thorough understanding of how porosity affects strength, ductility, and failure mechanisms.

Therefore, understanding how the resistance of porous materials depends on intrinsic aspects of the matrix material, such as metallurgical aspects of the dense metallic matrix in the case of powder metallurgy or even additive manufacturing, and on aspects such as geometry involving the geometry and distribution of pores, is of great importance for the safe design of porous components in critical engineering applications.

In this work, we present some preliminary results obtained by the computational homogenization of three-dimensional RVEs composed of randomly distributed, non-overlapping spherical voids embedded within an elastoplastic matrix. Different from most of the literature in the field, as for instance the works of Fritzen et al. [5, 6], Khdir et al. [7], da Maia et al. [8], here we allow that dense matrix (skeleton) of the RVE can experience isotropic hardening. The hardening model is given by a bounded Voce-type law. Based on the ideas presented by Fritzen et al. [5], distinct averaged macroscopic stress states are obtained by applying mixed boundary conditions and manipulating specific loading parameters. The obtained computational homogenization virtual data is presented in terms of graphs in the deviatoric-hydrostatic space showing the impact of the porosity level on the predicted macroscopic yield curves. This raw data will be used in further works to determine analytical pressure-sensitive macroscopic yield surfaces, such as those of Kuhn and Downey [9], Green [10], Gurson [11], Tvergaard and Needleman [12], Doraivelu et al. [13], among others. To achieve this objective, an appropriate fitting process must be developed to consider the data presented in this study.

The computational homogenization procedure described in this work was implemented inside the ABAQUS commercial software through an in-house PYTHON scripting interface, encompassing automatic pre- and post-processing. Also, the Voce-type hardening law was implemented in an UHARD user subroutine.

2 Theoretical background

In this work, quantities and fields related to the microscale RVE are marked with a tilde, that is $\tilde{\bullet}$, while quantities without a tilde must be understood as macroscopic quantities.

2.1 Averages

The macroscopic stress $\boldsymbol{\sigma}$ and strain $\boldsymbol{\varepsilon}$ are assumed to be approximated by the averages of the RVE microscopic stress and strain by

$$\sigma_{ij} = \frac{1}{\left|\tilde{\Omega}\right|} \int_{\tilde{\Omega}} \tilde{\sigma}_{ij} \, \mathrm{d}\tilde{\Omega}, \tag{1}$$

and

$$\varepsilon_{ij} = \frac{1}{\left|\tilde{\Omega}\right|} \int_{\tilde{\Omega}} \tilde{\varepsilon}_{ij} \, \mathrm{d}\tilde{\Omega}, \tag{2}$$

where $\left|\tilde{\Omega}\right|$ denotes the volume of the RVE.

The macroscopic von Mises equivalent stress and the macroscopic hydrostatic stress are calculated using

$$q = \sqrt{3J_2\left(\boldsymbol{\sigma}^{'}\right)} \tag{3}$$

and

$$p = \frac{1}{3} I_1\left(\boldsymbol{\sigma}\right), \tag{4}$$

respectively. Here the J_2 is the second invariant of the deviatoric stress $\boldsymbol{\sigma}^{'}$: $\boldsymbol{\sigma}^{'} = \boldsymbol{\sigma} - p\mathbf{I}$, while I_1 is the first invariant of the stress tensor[1].

2.2 RVE boundary conditions

Different stress triaxialities are used to evaluate the yield surface of the investigated microstructures. For this, mixed periodic boundary conditions are used. Alternative loading conditions are often used to control the triaxial ratio during loading, as seen in Besson et al. [14], Fritzen et al. [15], and Khdir et al. [16] just to cite a few. A variable general triaxiality results from the prescription of parameter values for coefficients α and β. For a time *t*, the following nominal macroscopic strains are imposed on the RVE

$$\begin{aligned} \varepsilon_{11}\left(t\right) &= t\dot{\varepsilon}\left(\alpha + \beta\right), \\ \varepsilon_{22}\left(t\right) &= t\dot{\varepsilon}\left(-\alpha + \beta\right), \\ \varepsilon_{33}\left(t\right) &= t\dot{\varepsilon}\beta, \end{aligned} \tag{5}$$

together with $\sigma_{ij} = 0$, $i \neq j$, ensuring that it is a macroscopic state free of shear stresses. Here $\dot{\varepsilon}$ is a prescribed reference rate of deformation and α and β are loading parameters in order to obtain distinct stress triaxialities.

Figure 1a illustrates a schematic representation of the strain imposition as described in eq. 5. Furthermore, Fig. 1b presents the RVE model, which includes multipores with an overall porosity of 30%, see 3 for more details.

2.3 Hardening model of the matrix

It is assumed that the material model of the matrix of the porous material could experience an isotropic hardening $\tilde{\kappa}$. Thus, the dense matrix follows a von Mises criteria expressed by the following yield function

[1] $J_2\left(\boldsymbol{\sigma}^{'}\right) = \frac{1}{2}\boldsymbol{\sigma}^{'} : \boldsymbol{\sigma}^{'}$ and $I_1 = \mathrm{tr}\left(\boldsymbol{\sigma}\right)$.

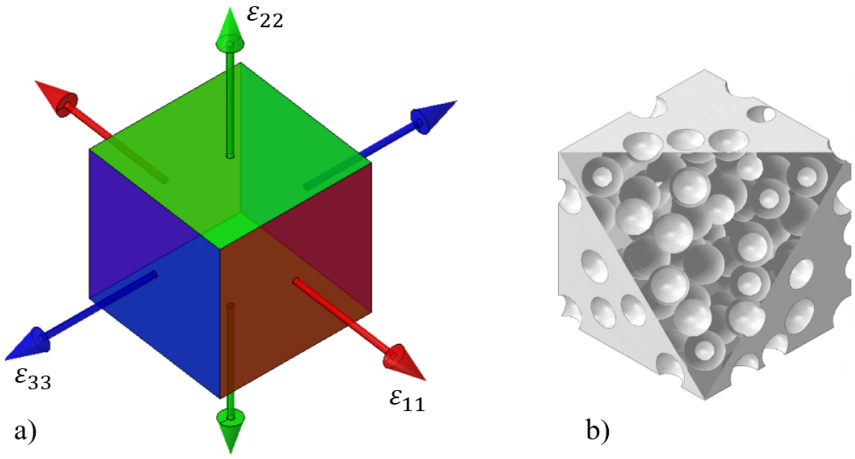


Figure 1. Imposition of the boundary condition on the RVE. a) schematic representation of eq. 5; b) multipores distribution with an overall porosity of 30%.

$$\tilde{f} = \tilde{q} - (\tilde{\sigma}_y + \tilde{\kappa}) \,, \tag{6}$$

where σ_y is the initial yield stress. By assuming a Voce-type of isotropic hardening

$$\tilde{\kappa}\left(\tilde{\epsilon}\right) = \left(\tilde{\sigma}_\infty - \tilde{\sigma}_y\right)\left(1 - e^{-\tilde{\delta}\tilde{\epsilon}}\right), \tag{7}$$

where the material parameters are the saturation stress (upper stress bound) $\tilde{\sigma}_\infty$ and $\tilde{\delta}$ a parameter that controls "how fast" the saturation is achieved. In this equations $\tilde{\epsilon}$ plays the role of the isotropic hardening strain (the accumulated plastic strain).

2.4 Relative density

A important parameter in the modeling of porous materials is the relative density or void volume fraction. Prior to advancing in the exposition of this work, we shall define relative density. The principle of mass conservation indicates that the evolution of mass density can be expressed as

$$\rho = \frac{\rho_0}{J}, \tag{8}$$

in which ρ_0 is the initial mass density and $J \equiv \det(\mathbf{F}) > 0$, $\mathbf{F}$ being the deformation gradient tensor. This equation can be presented in terms of the relative density η, which is defined as

$$\eta = \frac{\rho}{\rho_m} = \frac{\eta_0}{J}, \tag{9}$$

where ρ_m is the mass density of the fully dense material and $\eta_0 \equiv \frac{\rho_0}{\rho_m}$. Also, the relative density can be related to the void or pore volume fraction f by

$$\eta = 1 - f. \tag{10}$$

3 Modeling strategy

The effective mechanical response of a ductile porous metal is investigated using a three-dimensional RVE subject to computational homogenization. The RVE contains randomly distributed, non-overlapping spherical voids with volume fractions ranging from 1% to 30%. Spatial periodicity of the pore arrangement is enforced by using the open-source Mote3D Richter [17], see Fig 1b. The matrix is modeled as an isotropic elastic and isotropic hardened plastic material. The elastic material parameters are Young's modulus $\tilde{E} = 200$ GPa and Poisson's ratio $\tilde{\nu} = 0.3$. In this work, the material parameters that define the initial yielding and isotropic hardened plastic behavior are: $\tilde{\sigma}_y = 100$ MPa, $\tilde{\sigma}_\infty = 150$ MPa, and $\tilde{\delta} = 30$.

3.1 Computational homogenization

Macroscopic stresses are obtained by volume averaging the microscopic stress field in the RVE, see e.g. Zohdi and Wriggers [18]. In practice, the Abaqus finite element implementation is used with the integration-point volume (IVOL) option. Thus, the components of the average (macroscopic) stress tensor in eq. 1 are computed as

$$\sigma_{ij} = \frac{1}{\left|\tilde{\Omega}\right|} \int_{\tilde{\Omega}} \tilde{\sigma}_{ij} \, \mathrm{d}\tilde{\Omega} \approx \frac{1}{\left|\tilde{\Omega}^h\right|} \sum_{\xi=1}^{n} \tilde{\sigma}_{ij}\left(\tilde{\xi}\right) \, \mathrm{IVOL}\left(\tilde{\xi}\right), \tag{11}$$

where $\tilde{\sigma}_{ij}\left(\tilde{\xi}\right)$ is the microscopic stress at integration point $\tilde{\xi}$, n is the total number of Gauss points, and $\left|\tilde{\Omega}^h\right|$ is the FEM discretized RVE volume. Equation (11) follows from the finite element approximation of the RVE domain, and ensures that the macroscopic stress is the volume average of the microscopic stresses. In this work all averages are taken in the undeformed (reference) configuration, but the stresses σ_{ij} are taken in the current (updated) configuration.

The specific combination of the parameters α and β, see eq. 5, used in this study are given in Table 1[1].

Table 1. Loading parameters α and β for each test case

Case	1	2	3	4	5	6	7	8	9
α	1	1	1	1	1	1	1	0.5	0
β	0	0.05	0.1	0.15	0.25	0.5	1	1	1

4 Numerical results

4.1 Macroscopic hardening surfaces from virtual tests

This subsection presents the numerical results obtained from the application of the computational homogenization model described in Section 2 and 3, considering Voce hardening in the metallic matrix. The objective is to characterize the macroscopic yield surfaces by varying the porosity and hardening parameters.

Virtual tests were carried out on three-dimensional RVEs containing non-overlapping hollow spheres, with a pore volume of 30%. Figure 2 shows two results in the space $p \times q$ considering the multiple pores example as depicted in Fig. 1b. The first one, in dotted lines, shows the macroscopic yield curve for a material considering the elastic-perfectly plastic matrix. The curve in continuous lines shows the macroscopic yield surface for a material considered isotropic hardening. Note the increase in the apparent elastic region between the two cases. Also, notice the differences in the stress path until asymptotic behavior is reached.

Note that both the dotted and the solid black line shown in Fig. 2 represent only a linear interpolation of the near-asymptotic macroscopic points of p and q.

Figure 3 shows the macroscopic yield surfaces obtained from virtual tests for a varying porosity from 1% to 30% considering multiple pores. In this figure, dotted lines are the results for elastic-perfectly plastic material, while the continuous lines are the results for hardened matrix again for $\tilde{\sigma}_\infty = 150$ MPa and $\tilde{\delta} = 30$ in eq. 7.

[1] Refer to da Maia et al. [19] for a smoother curve, that is, with more triaxial loading cases.

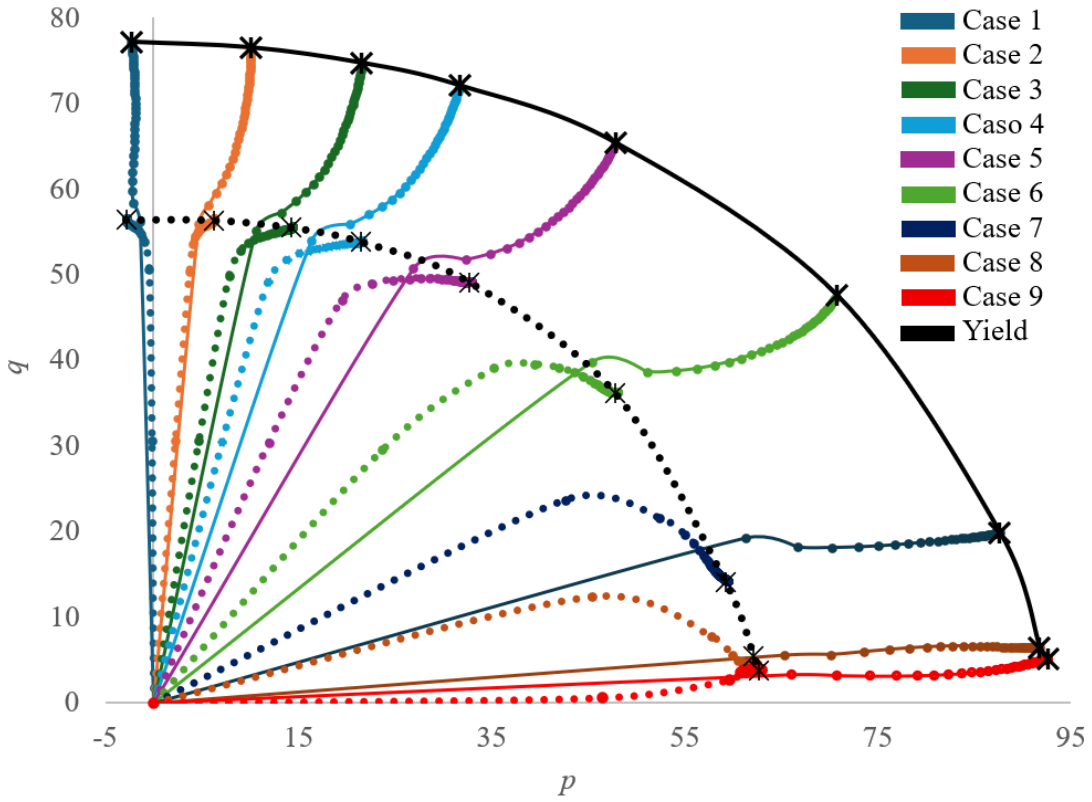


Figure 2. Macroscopic yield surfaces obtained from virtual tests for a porosity of 30% and considering multiple pores. Dotted lines: elastic-perfectly plastic material; Continuous lines: Hardened matrix with $\tilde{\sigma}_\infty = 150$ MPa and $\tilde{\delta} = 30$ in eq. 7.

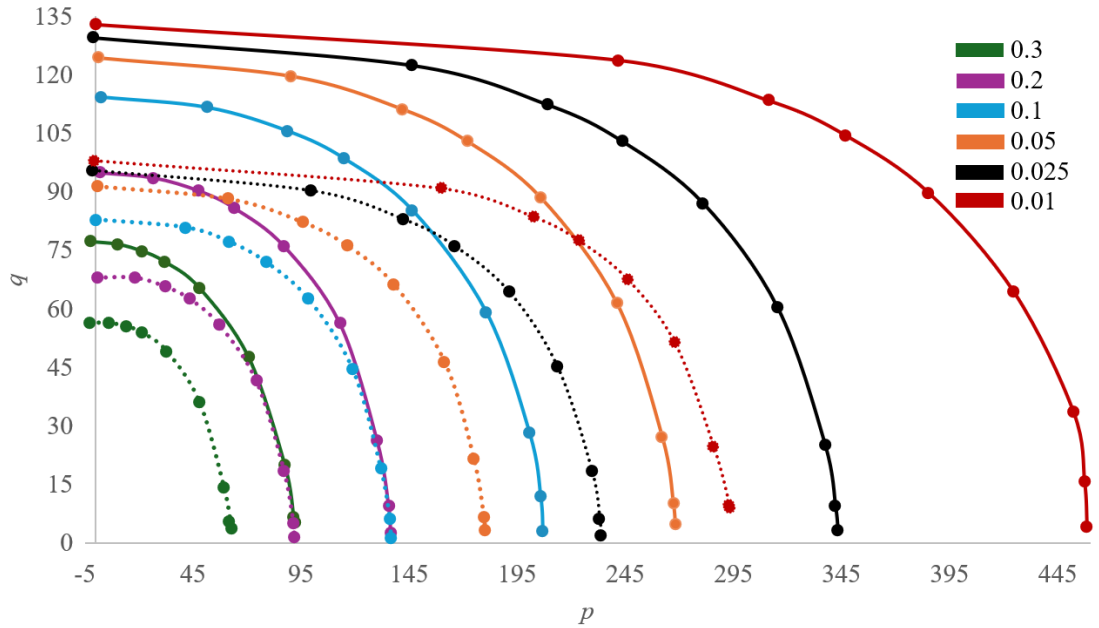


Figure 3. Macroscopic yield surfaces varying porosity from 1% to 30% and considering multiple pores. Dotted lines: results for elastic-perfectly plastic material; Continuous lines: results for hardened matrix again for $\tilde{\sigma}_\infty = 150$ MPa and $\tilde{\delta} = 30$ in eq. 7

5 Conclusions

This study investigated the mechanical behavior of porous metallic materials using three-dimensional computational homogenization based on Representative Volume Elements (RVEs), with a particular focus on capturing macroscopic hardening behavior via a bounded Voce-type isotropic hardening J_2 plasticity associated with the matrix of the RVE. By embedding non-overlapping spherical voids in an elastoplastic matrix and performing virtual tests under multiple triaxial loading paths, a dataset of macroscopic stress responses was generated.

The use of virtual tests with 3D computational homogenization allowed the construction of macroscopic yield surfaces for porous materials with different triaxialities and porosity levels. The results demonstrate that the Voce hardening introduces a non-trivial evolution of the apparent strength, strongly modulated by porosity and void distribution. The adopted approach offers a solid basis for calibrating phenomenological constitutive models, with greater fidelity to the actual responses expected from components produced by additive manufacturing or powder metallurgy. This research will proceed in two parts: first, to obtain results by varying the isotropic hardening parameters $\tilde{\sigma}_\infty$ and $\tilde{\delta}$; second, to identify macroscopic yield functions that accurately represent the behavior of hardening porous materials.

Acknowledgements. The authors gratefully acknowledge the financial support of the Brazilian National Council for Scientific and Technological Development (CNPq) through Productivity Grant No. 302581/2025-1 awarded to Rodrigo Rossi and Doctoral Scholarship No. 163058/2022-9 granted to Carlos Alberto da Maia.

Authorship statement. The authors hereby confirm that they are the sole liable persons responsible for the authorship of this work, and that all material that has been herein included as part of the present paper is either the property (and authorship) of the authors, or has the permission of the owners to be included here.

References

[1] P. Liu and G.-F. Chen. *Porous materials: processing and applications*. Elsevier, 2014.
[2] J. Banhart, J. Baumeister, and M. Weber. Metal foams near commercialization. *Metal Powder Report*, vol. 53, pp. 38, 1997.
[3] A. Binder C., I. C. M. Lenzi, Mocellin, R. P, and Becker. Processo de fabricação de um corpo poroso, por metalurgia do pó e composição metalúrgica de materiais particulados. Instituto Nacional da Propriedade Industrial RPI2235, 2013.
[4] M. Ahmed Obeidi, S. M. Uí Mhurchadha, R. Raghavendra, A. Conway, C. Souto, D. Tormey, I. U. Ahad, and D. Brabazon. Comparison of the porosity and mechanical performance of 316l stainless steel manufactured on different laser powder bed fusion metal additive manufacturing machines. *Journal of Materials Research and Technology*, vol. 13, pp. 2361–2374, 2021.
[5] F. Fritzen, S. Forest, T. Böhlke, D. Kondo, and T. Kanit. Computational homogenization of elasto-plastic porous metals. *International journal of plasticity*, vol. 29, pp. 102–119, 2012a.
[6] F. Fritzen, S. Forest, D. Kondo, and T. Böhlke. Computational homogenization of porous materials of green type. *Computational Mechanics*, vol. 52, n. 1, pp. 121–134, 2013.
[7] Y. Khdir, T. Kanit, F. Zaïri, and M. Naït-Abdelaziz. Computational homogenization of elastic–plastic composites. *International journal of solids and structures*, vol. 50, n. 18, pp. 2829–2835, 2013.
[8] da C. A. Maia, A. Brezolin, dos T. Santos, and R. Rossi. An implementation of 3d rve-based computational homogenization considering an elastic-perfectly plastic matrix and spherical voids, 2022.
[9] H. Kuhn and C. Downey. Deformation characteristics and plasticity theory of sintered powder metals. *Int. J. Powder Mat.*, vol. 7, 1971.
[10] R. Green. A plasticity theory for porous solids. *International Journal of Mechanical Sciences*, vol. 14, n. 4, pp. 215–224, 1972.
[11] A. L. Gurson. Continuum theory of ductile rupture by void nucleation and growth: Part i—yield criteria and flow rules for porous ductile media, 1977.
[12] V. Tvergaard and A. Needleman. Analysis of the cup-cone fracture in a round tensile bar. *Acta metallurgica*, vol. 32, n. 1, pp. 157–169, 1984.
[13] S. Doraivelu, H. Gegel, J. Gunasekera, J. Malas, J. Morgan, and J. Thomas Jr. A new yield function for compressible pm materials. *International Journal of Mechanical Sciences*, vol. 26, n. 9-10, pp. 527–535, 1984.
[14] J. Besson, C. Berdin, S. Bugat, F. Feyel, S. Forest, and A. Pineau. *Local approach to fracture*. Science de la matière. Presse des Mines, 2004.

[15] F. Fritzen, S. Forest, T. Böhlke, D. Kondo, and T. Kanit. Computational homogenization of elasto-plastic porous metals. *International Journal of Plasticity*, vol. 29, pp. 102–119, 2012b.
[16] Y.-K. Khdir, T. Kanit, F. Zaıri, and M. Naıt-Abdelaziz. A computational homogenization of random porous media: Effect of void shape and void content on the overall yield surface. *European Journal of Mechanics - A/Solids*, vol. 49, pp. 137–145, 2015.
[17] H. Richter. Mote3d: An open-source toolbox for modelling periodic random particulate microstructures. *Modelling and Simulation in Materials Science and Engineering*, vol. 25, 2017.
[18] T. I. Zohdi and P. Wriggers. *An introduction to computational micromechanics*, volume 20. Springer Science & Business Media, 2004.
[19] da C. A. Maia, A. Brezolin, and R. Rossi. Virtual homogenization tests on porous materials using 3d rves. pp. 140–154, 2024.